Lattice approach for $\alpha+H_2^+$ collisions

S. C. Cheng and B. D. Esry
Department of Physics and J. R. Macdonald Laboratory, Kansas State University, Manhattan, Kansas 66506, USA
(Received 2 November 2004; published 9 August 2005)

We solve the time-dependent Schrödinger equation for an ion-molecule collision using a lattice approach. This method carries over naturally from similar lattice treatments of ion-atom collisions, and is free from the multicenter problems that make extensions of other ion-atom methods difficult.

DOI: 10.1103/PhysRevA.72.022704 PACS number(s): 34.50.−s, 34.10.+x

I. INTRODUCTION

Charge-transfer processes in ion-atom collisions have been studied for many years and are relatively well understood [1,2]. Ion-molecule collisions, on the other hand, are not yet so well understood. The major difficulty, of course, is that ion-molecule collisions have many more degrees of freedom. Theoretically, the difficulty is often labeled the multicenter problem, and limits the straightforward adaptation of many of the successful ion-atom methods to ion-molecule collisions. While progress has been made [4], it has been slow in coming.

In this work, we will describe one method, successful for ion-atom collisions, that can be simply adapted to ion-molecule collisions. That method is the lattice solution of the time-dependent Schrödinger equation (see, for example, Refs. [5–7] for applications to ion-atom collisions). Since there are no integrals to be evaluated in the lattice approach, the multicenter nature of molecular targets poses few numerical difficulties beyond those already present for atomic targets. In both cases, the Coulomb singularities in the electron-nuclear interactions require careful treatment in the lattice approach. While some calculations simply guarantee that the singularities always fall between lattice points [5,6], we choose instead to introduce a softening parameter into the Coulomb potential.

We will illustrate the application of the method with the collision of an α particle with H_2^+. This system has recently been studied experimentally by Reiser *et al.* [8,9] and by Bräuning *et al.* [10]. The main observation in Refs. [8,9] was that charge transfer is favored when the molecule is perpendicular to the α beam.

There have been other theoretical treatments of ion-molecule collsions. Kimura *et al.*, for instance, have studied $H^+ + H_2$ [11] and $Ar^+ + H_2$ [12] collisions using a molecular orbital, close-coupling approach. A similar approach has been used more recently by Caillat *et al.* to study $\alpha+H_2^+$ [14]. Coupled channels have also been recently employed by Krstić *et al.* to study the collisions $H^+ + H_2$ and $H + H_2^+$ below about 10 eV [13,14]. Less sophisticated methods have also been used: Tuan and Gerjuoy, for instance, used the first Born approximation and represented the molecular target with a simple linear combination of atomic orbitals [15]. McGuire *et al.* [16,17] developed this idea further, and Shingal and Lin [18,19] adapted the idea to use accurate scattering amplitudes from ion-atom calculations.

II. THEORY

We base our treatment on the usual semiclassical, impact parameter approach used so succesfully for ion-atom collisions [2]. The target, of course, requires extra consideration. For high collision velocities, such that the typical collision time is much shorter than the vibrational and rotational time scales of the target H_2^+, we can simply treat the protons as fixed during the collision, carrying out appropriate averages after the fact. Similar procedures have long been used in molecular collisions, and the validity of these kinds of approximations have been investigated (see, for example, Ref. [3]). For the velocity used here—$v_\alpha = 0.41$ a.u., chosen for easy comparison with experiment [8,9]—the collision time is roughly an order of magnitude smaller than the H_2^+ ground-state vibrational period. Fixing the nuclei is thus a reasonable approximation for this collision velocity. So, we need only solve for the electronic degrees of freedom just as in ion-atom collisions.

The time-dependent electronic Schrödinger equation (TDSE) for the $\alpha+H_2^+$ system is (in atomic units)

$$i\frac{\partial}{\partial t}\psi(\mathbf{r},t) = H\psi(\mathbf{r},t). \tag{1}$$

Figure 1 shows the coordinate system we used. The origin of the electronic coordinates is placed at the center of mass of the two protons, and $\mathbf{r}$ indicates the position of the electron. The electronic Hamiltonian H is given by

$$H = -\frac{1}{2}\nabla^2 - \frac{Z_\alpha}{|\mathbf{r}_\alpha - \mathbf{r}|} - \frac{Z_A}{|\mathbf{r}_A - \mathbf{r}|} - \frac{Z_B}{|\mathbf{r}_B - \mathbf{r}|} \tag{2}$$

where $\mathbf{r}_i (i = \alpha, A, B)$ are the positions of the heavy particles, and Z_i their charges. The internuclear distance $\mathbf{R}$ for the target includes, in principle, all three spherical coordinates, but

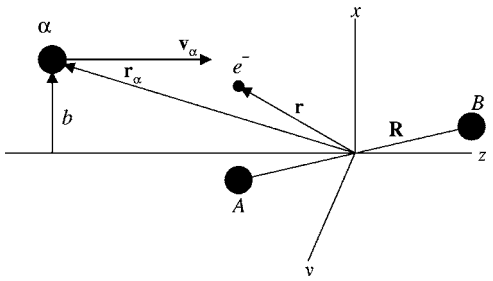

FIG. 1. The coordinate system.

we actually rotated the α particle by the azimuthal angle ϕ (keeping H_2^+ in the xz plane) to simplify the calculations.

Each solution of the TDSE will produce a probability that depends on five parameters—$\mathbf{R}$, b, and v_α—through the heavy-particle positions $\mathbf{r}_i$ in H. The three extra parameters $\mathbf{R}$ arise, of course, from the fact that the target is a molecule. Depending on the nature of the results sought, one or all of these parameters will need to be integrated over. Such integrals require several points in each parameter to evaluate with any accuracy, increasing the computational demands of the calculation.

For the present comparisons, we note that the experimental measurements of Reiser *et al.* were performed at fixed collision energies and are differential in the angle θ. We will thus integrate over ϕ and b, but will set R at a few characteristic values since we only seek here to illustrate the lattice approach. The resulting quantity

$$\sigma_{\mathrm{cap}}(R,\theta,v_\alpha) = \int b\, db \int d\phi\, P_{\mathrm{cap}}(\mathbf{R},b,v_\alpha) \tag{3}$$

is the differential capture cross section at an internuclear distance R. For proper comparison with experiment, σ_{cap} should be averaged over R weighted by the initial R distribution. In the present case, H_2^+ was produced in the experiment from H_2 in an ion source, yielding H_2^+ with approximately a Franck-Condon distribution of vibrational states. Note that we assume a ϕ-independent initial distribution of nuclear alignments, but a particular distribution could, in principle, be included in Eq. (3).

The capture probability P_{cap} in Eq. (3) can be obtained, for instance, by projecting the total wave function at large times onto the bound states of the projectile. This procedure would yield state-specific capture cross sections if such measurements are available for comparison. It is also possible to calculate excitations of the target by similar projections onto the molecular target states. In the present case, however, with a H_2^+ target, all electronic excitations lead to dissociation into $p+\mathrm{H}$. These channels were cleanly separated experimentally [8,9] from the capture channel by requiring $p+p$ coincidences.

III. NUMERICAL METHOD

A. Algorithm

The short description of the time propagation is that we discretized the three-dimensional Cartesian coordinates on uniform grids, approximated kinetic energy operators using three-point finite differences, and used a split-operator, Crank-Nicholson propagation scheme [20]. Since the latter can be implemented in many ways, though, we will provide some details. The wave function can be advanced in time using the short-time evolution operator:

$$\psi(\mathbf{r},t+\delta) \approx e^{-iH\delta}\psi(\mathbf{r},t). \tag{4}$$

We use a symmetric splitting of the exponential to preserve the accuracy and unitarity of the evolution,

$$e^{-iH\delta} \approx e^{-iV\frac{\delta}{2}} e^{-iT_x\delta} e^{-iT_y\delta} e^{-iT_z\delta} e^{-iV\frac{\delta}{2}}. \tag{5}$$

In this expression, $T_j (j=x,y,z)$ are the kinetic energy operators whose exponential can be put in this simple form since they commute, and V is the sum of all electron-nuclear Coulomb interactions from Eq. (2). This separation has the added benefit of allowing each direction to be updated independently. The three-dimensional propagation is thus reduced to repeated applications of one-dimensional propagators—a property shared by most successful multidimensional time evolution schemes. Note that we split H as $V/2+T+V/2$ rather than as $T/2+V+T/2$ since the exponential of the kinetic energy T is more costly to evaluate. The one-dimensional updates are handled using the Cayley form,

$$e^{-iT_j\delta} \approx \frac{I - iT_j\frac{\delta}{2}}{I + iT_j\frac{\delta}{2}}, \tag{6}$$

so that the updated wave function is found from the solution of the linear equations

$$\left(I + iT_j\frac{\delta}{2}\right)\psi(t+\delta) = \left(I - iT_j\frac{\delta}{2}\right)\psi(t). \tag{7}$$

(The symbol I represents the unit matrix.) This procedure amounts to the familiar Crank-Nicholson algorithm since we evaluate the kinetic energy with three-point finite differences, requiring tridiagonal linear solves for Eq. (7). All of the approximations detailed above give the same order for the leading error in time, namely, $O(\delta^3)$.

The potential is a diagonal matrix on the grid, so its exponential can be evaluated exactly. Since the other exponentials are only accurate to order δ^2, however, we can gain some computational efficiency by evaluating the potential term to the same order

$$e^{-iV\frac{\delta}{2}} \approx \frac{I - iV\frac{\delta}{4}}{I + iV\frac{\delta}{4}}. \tag{8}$$

There will naturally be numerical problems if one of the three Coulomb singularities in V falls on a grid point. By the same token, there are problems when the singularity of the Coulomb potential for the projectile moves through the grid along the fixed, straight-line trajectory. The electron effectively sees an oscillating potential as the singularity approaches and recedes from grid points. There are different ways to minimize this effect, and we have chosen to add a soft core to each of the electron-nuclear Coulomb potentials,

$$V_C(x,y,z) = -\frac{Z}{\sqrt{x^2+y^2+z^2+a^2}}. \tag{9}$$

In this expression, a is a small parameter that eliminates the Coulomb singularity. Such soft-core Coulomb potentials are commonly used in one-dimensional calculations to remove the singularity. When the soft-core parameter a is chosen

correctly, the modified Coulomb potential, Eq. (9), no longer oscillates as it moves through the grid—or at least the oscillation is reduced to a level that can be neglected. Adding a worsens the representation of the energy spectrum, however. States with low orbital angular momentum will be shifted from the exact results, for instance, more than those with higher angular momentum, breaking their degeneracy. A compromise must therefore be struck between softening the Coulomb potential and representing its spectrum accurately.

A compromise must also be struck between the size of the grid and the computational time. The physics of the present system dictates a grid large enough to contain both the target and projectile states for all times during the collision, and long enough after the collision to be able to clearly distinguish between capture and excitation. But the CPU time scales like $N_xN_yN_z$ where N_j is the number of grid points in the direction j. We seek, then, the smallest grid that represents the physics we are interested in. Fortunately, in the present problem, we are interested only in the total capture probability. We need not struggle to represent the projectile states for long after the collision—we can have a grid just large enough to contain the interaction region.

Since the total wave function is not represented for all times during the calculation, there must be a mechanism for eliminating selected portions of it. Time-dependent calculations, however, have long utilized absorbing boundaries to eliminate unphysical reflections from the edge of the grid. We will use the same technique to absorb the portion of the wave function corresponding to capture. Whatever fraction of the total probability density remains on our computational grid long after the projectile has passed (and passed off the grid) gives us the information we seek. Explicitly,

$$P_{\mathrm{cap}}(\mathbf{R},b,v_\alpha) = 1 - \int_{\mathrm{grid}} |\psi(\mathbf{r},t\to\infty)|^2 dV. \tag{10}$$

Strictly speaking, this is the total probability for capture plus ionization, but, as stated above, we can neglect ionization for the projectile velocity of interest here. In practice, the integration only needs to be carried out to a large enough time such that the probability Eq. (10) converges to a desired accuracy.

Absorbing boundaries can be implemented in a number of ways (optical potentials and nonlocal boundary conditions, for instance), but we chose to use masking functions. A masking function is unity over most of the grid, but decreases near the edges. At each time step, the wave function is multiplied by the masking function, thus eliminating those portions of the wave function near the edge of the grid. In fact, a masking function is equivalent to an imaginary potential that is zero over most of the grid and nonzero near the edges. We use a masking function of the form

$$M(x) = \begin{cases} \exp\left[-\left(\dfrac{x-x_L}{d}\right)^2\right], & x_{\min} \leqslant x \leqslant x_L, \\ 1, & x_L < x < x_R, \\ \exp\left[-\left(\dfrac{x-x_R}{d}\right)^2\right], & x_R \leqslant x \leqslant x_{\max}, \end{cases} \tag{11}$$

where the quantity $x_{\min}(x_{\max})$ is the minimum (maximum) value of the grid and $x_L(x_R)$ is the beginning (ending) point of the physical part of the grid. Note that it is not necessary for $M(x)$ to be zero at the grid boundaries. In fact, for computational efficiency, $M(x)$ should not be zero at the edge, because this allows the fraction of the grid devoted to the masking region to be minimized. The masking function should change smoothly from unity so that it does not introduce any unphysical reflections. The exact values of the parameters x_L, x_R, and d need to be determined from numerical testing. The total three-dimensional masking function is then simply a product of the one-dimensional function $M(x)$,

$$M(x,y,z) = M(x)M(y)M(z). \tag{12}$$

B. Validation and convergence

There are a number of parameters that influence these calculations: the soft-core parameter, the masking function parameters, the spatial grid steps and sizes, and the temporal step size. Again, since our goal is the qualitative dependence of the capture cross section on molecular alignment, we can accept errors that would otherwise be relatively large. Our *a priori* goals were to reproduce the energy spectra of the atoms and molecules at the 10% level, then to solve the resulting model at the 1% level.

Relatively general physical considerations dictate that the range of the grid should be tens of atomic units; practical computational limitations dictate that the number of grid points be in the hundreds for each dimension. Consequently, the spatial step size must be on the order of 0.1 a.u. This value is not unreasonable for representing atomic wave functions, and our testing began with a grid spacing of $\Delta x = 0.2$ a.u. and a grid range of $x_{\min} = -18$ a.u. to $x_{\max} = 18$ a.u. These values were the same for each coordinate.

To determine the value of the soft-core parameter a, we must balance the representation of the energy spectrum with the problems of moving Coulomb singularities. Further, the optimal value of a will depend on the time and space grid parameters. To take all of these factors into account, we chose a by seeking the smallest value that preserved energy conservation to 1% for an electron moving along with a proton whose velocity was 0.41 a.u. For a grid spacing of $\Delta x = 0.2$ a.u., we found that $a = 0.134$ a.u. maintains the expectation value of the energy at -0.378 a.u. to two digits for the whole propagation. The time step was $\delta = 0.06$ a.u. and the proton traveled from one edge of the grid to the other. This choice of a yields a hydrogen ground state energy of -0.454 a.u. which is within our error goal of 10% for energies. We use the same value of a in all of the Coulomb potentials.

The soft-core will necessarily affect the representation of the electronic states of the H_2^+ target. To see the effect, we plot in Fig. 2 the Born-Oppenheimer potential calculated using the above grid and soft core. We find that the equilibrium internuclear distance lies at $R = 2.2$ a.u. which is in error by about 10% when compared with accurate calculations. On the other hand, the dissociation energy from the minimum of the potential is 0.101 a.u. which differs from the accurate value of 0.103 a.u. by only about 2%. Note that the soft core ensures that this potential curve will be the same to about 1% no matter the molecular alignment.

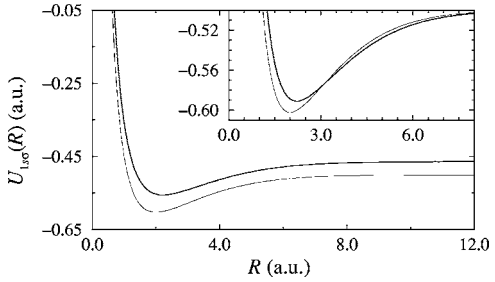

FIG. 2. The $1s\sigma$ Born-Oppenheimer potentials for H_2^+: the heavy line is calculated with the present lattice approach and the light line is an accurate solution. The inset compares the shape of the two potentials by shifting the present result to give the correct asymptotic threshold.

We must also determine the parameters for the masking function. With the grid and soft-core parameters as above, we found good results when $x_L=-13$ a.u. and $x_R=13$ a.u. with $d=5.94$ a.u. These values make $M(x_{\min})=M(x_{\max})=0.5$ and reproduce the probability density within the physical region x_L to x_R to two digits when compared with calculations on larger grids. The validation test just mimicked the full collision calculation: we sent a proton through the grid at $v=0.41$ a.u. with the electron attached and ran it into the edge of the grid. A successful masking function, in this case, is one that leaves zero total probability on the grid after the proton is off the grid. In the full calculation, the remaining portion tells us the total capture probability via Eq. (10).

To check that all of the above approximations do not adversely affect the computation of the total capture probability, we applied our method to the canonical system p+H since a considerable amount of reliable data exists for comparison. The resulting P_{cap} [analyzed using Eq. (10)] as a function of impact parameter for a collision velocity of 0.447 a.u. is shown in Fig. 3. For comparison, we also show the results from Shingal and Lin [19]. There is reasonable agreement between them, especially given our previously stated error estimates. In fact, the present cross section is only about 5% higher.

Next, we should verify that the final results are sufficiently converged with respect to the space and time steps. For these tests, we will use $\alpha+H_2^+$ with the target at the fixed orientation $\theta=90°$, $\phi=0°$, and internuclear distance

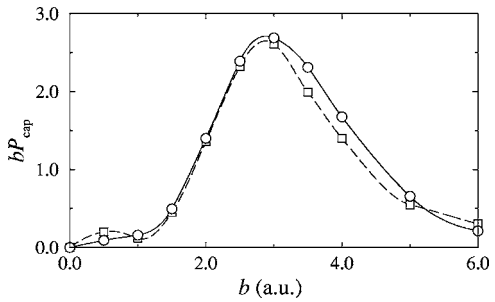

FIG. 3. The total electron capture probability as a function of impact parameter b for p+H at an impact energy of 5 keV ($v_p=0.447$ a.u.). The circles mark the results from the present lattice approach; and the squares, accurate calculations from Ref. [19].

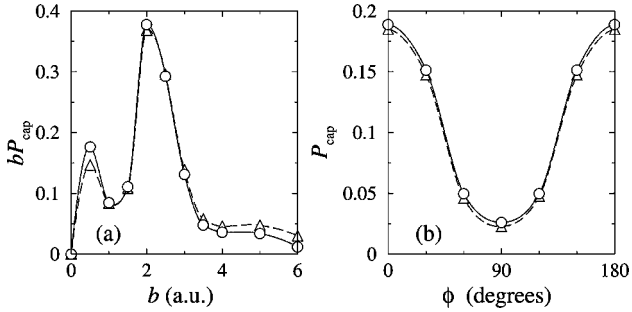

FIG. 4. Convergence tests for the electron capture probability for $\alpha+H_2^+$. In (a), $\delta=0.06$ a.u. and $\phi=0°$; the circles mark $\Delta x=0.2$ a.u. while the triangles mark $\Delta x=0.1$ a.u. In (b), $\Delta x=0.2$ a.u. and $b=2.0$ a.u.; the circles mark $\delta=0.06$ a.u. while the triangles mark $\delta=0.03$ a.u. The other parameters are $v_\alpha=0.41$ a.u., $R=2.2$ a.u., and $\theta=90°$.

$R=2.2$ a.u. The results for $P_{\text{cap}}(b)$ with $\Delta x=0.2$ a.u. and $\Delta x=0.1$ a.u. are shown in Fig. 4(a). The integral over b for these two curves differs by only 2.9%, but the CPU time is roughly a factor of 8 larger for $\Delta x=0.1$ a.u. Since the shorter calculation already takes 11 hours on our 2 GHz Pentium 4 Xeon workstation, we can accept this level of inaccuracy. Figure 4(b) shows the results of halving the time step δ from $\delta=0.06$ a.u. Again, the target was held fixed at $R=2.2$ a.u. and $\theta=90°$, and $b=2.0$ a.u.; the integrated capture probability over ϕ differed by only a few percent (3.6%).

IV. RESULTS AND DISCUSSION

As discussed in Sec. II, the electron capture probability depends on the internuclear distance R, the projectile velocity v_α, the angles θ and ϕ, and the impact parameter b. Since it takes about 11 h to run each set of parameters, we want to determine the fewest number of points needed for each of these parameters while maintaining our $\sim$1% accuracy goal.

Since b and ϕ are the only parameters that will actually be integrated over, it is most important to insure faithful reproduction of their behavior. From studying many plots of P_{cap} as a function of b and ϕ, we find that we can use ten points for b and six points for ϕ and maintain our accuracy goal for the integrated capture probability.

It is reasonable to begin the study of this collision system with H_2^+ fixed at its equilibrium internuclear distance. Figure 5 shows the differential capture cross section $\sigma(R,\theta,v_\alpha)$ as a function of θ for H_2^+ at its equilibrium distance in our model, $R=2.2$ a.u. Figure 5 shows that electron capture is more likely when the molecule is aligned with the α beam than when it is perpendicular to it. This behavior is just the opposite of that observed in the experiment of Reiser *et al.* [8,9].

One possible source of this disagreement is that the H_2^+ was produced experimentally by stripping H_2, so the initial R distribution will be determined by a vertical transition from the H_2 ground state. Figure 6 shows the capture cross section at $R=1.4$ a.u., the equilibrium distance for H_2. At this distance, capture is even more strongly favored at 0° and 180° than in Fig. 5.

We repeated the calculations at several values of R between the equilibrium distances of H_2 and H_2^+. The results

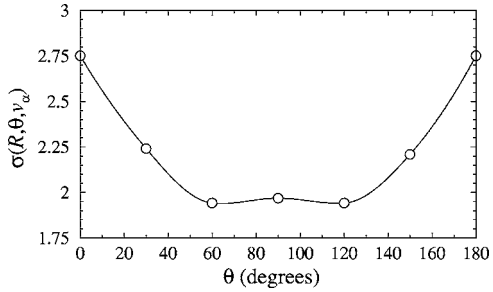

FIG. 5. The differential capture cross section $\sigma(R,\theta,v_\alpha)$ Eq. (3) as a function of θ at $R=2.2$ a.u., the equilibrium of H_2^+ in our model (see Fig. 2).

are shown in Fig. 7 (note that each point represents 60 individual calculations). A few features are apparent. First, each differential capture cross section has the same qualitative behavior so that an average over these internuclear distances (using, for instance, Franck-Condon weighting) would yield a cross section with the same behavior. Second, the region near $\theta=90°$ is flattening slightly as R increases. Third, the overall magnitude of the cross section is increasing with R, decreasing the relative difference between 0° and 90°.

Some qualitative understanding of these results and a possible route to reconciling the present results with experiment can be gained from considering the interference model of Shingal and Lin [18,19]. They found that the amplitude **a** for capture from the ground state of H_2^+ could be written as

$$\mathbf{a} = \frac{1}{\sqrt{2}}[\mathbf{a}(\mathbf{b}_A) + \mathbf{a}(\mathbf{b}_B)e^{-iR\cos\theta\left(\frac{v}{2}-\frac{\omega}{v}\right)}] \tag{13}$$

where $\mathbf{a}(\mathbf{b}_A)$ and $\mathbf{a}(\mathbf{b}_B)$ are the capture amplitudes from the H atoms at the impact parameters $\mathbf{b}_A$ and $\mathbf{b}_B$; v is the projectile velocity; and ω is the energy difference between the initial and final states. Similar expressions were obtained in Refs. [15–17]. The capture probability is thus

$$P = \frac{1}{2}\{|\mathbf{a}_A|^2 + |\mathbf{a}_B|^2 + 2\,\mathrm{Re}[\mathbf{a}_A^*\mathbf{a}_B e^{-i\Phi}]\} \tag{14}$$

using a shorthand notation for the atomic amplitudes and defining the phase

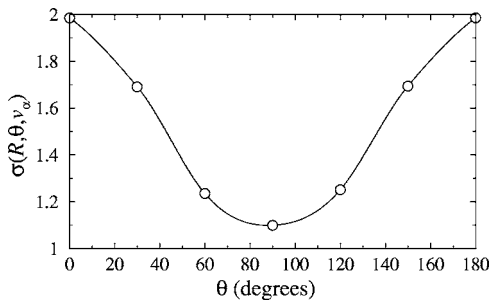

FIG. 6. The differential capture cross section $\sigma(R,\theta,v_\alpha)$ Eq. (3) as a function of θ at $R=1.4$ a.u., the equilibrium value of H_2.

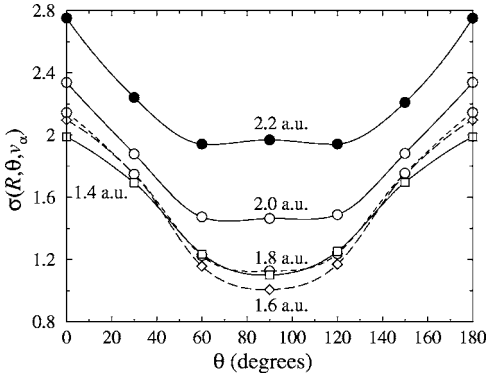

FIG. 7. The differential capture cross section $\sigma(R,\theta,v_\alpha)$ Eq. (3) as a function of θ at several values of R: 1.4 a.u. (squares and solid line), 1.6 a.u. (diamonds and dashed line), 1.8 a.u. (circles and dashed line), 2.0 a.u. (circles and solid line), and 2.2 a.u. (filled circles and solid line).

$$\Phi = R\cos\theta\left(\frac{v}{2}-\frac{\omega}{v}\right). \tag{15}$$

Setting aside any contributions from the atomic scattering amplitudes themselves, we see that there is an interference due, in some sense, to the differing path lengths for capture from each center. This interference is determined in this simple model by the phase Φ which is proportional to R. So, holding everything else fixed, one can expect that the capture probability will oscillate as a function of R, making it possible for the behavior displayed in Fig. 7 to reverse itself as R is increased beyond the values calculated here. This reversal may be sufficient to bring the calculation into agreement since about 60% of the Franck-Condon distribution lies at R values larger than 2.2 a.u. Whether this does, in fact, happen is being explored by another group [21] as is the velocity dependence.

The increase in the overall magnitude of the cross section can also be understood from Eq. (14) and Fig. 8. Figure 8 shows the capture probability for $\alpha+H$ calculated with the same lattice approach used for the molecular target, but for a slightly higher velocity. Since the capture probability extends to quite large impact parameters, Eq. (14) says that the molecule simply presents an increasingly larger target as R increases—while $P_{\mathrm{cap}}(b)$ from each center still overlaps. For

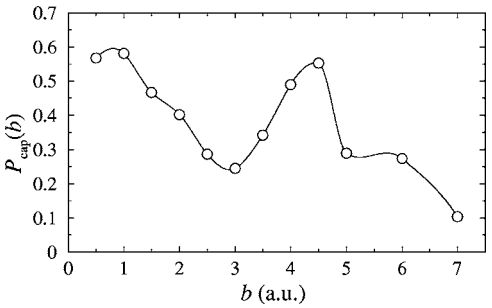

FIG. 8. The total electron capture probability as a function of impact parameter b for $\alpha+H$ at $v_\alpha=0.477$ a.u. calculated with the the present lattice approach.

larger R, the atomic capture cross sections will be recovered. Again, weighting with the initial R distribution will be important for comparison with experiment.

V. SUMMARY

We have presented a lattice solution of the time-dependent Schrödinger equation for the collision of an ion with a molecule. As an example, the method was applied to the collision of $\alpha+H_2^+$ and found to give qualitatively different results than experiment for the limited parameters studied. More extensive studies are beyond the purposes of this paper and are being undertaken by Phalen, Pindzola, and Robicheaux [21].

The lattice approach is free from the multicenter difficulties that make extensions of other methods problematic. The necessity of averaging over target parameters makes calculations rather costly which, in turn, elevates the importance of planning to minimize the computational effort where possible. This averaging was, of course, a consequence of our approximations for the motion of the heavy particles which limits our treatment to higher collision energies. On the other hand, the lattice approach does not bias the solution in ways that other methods do, providing an avenue to check simpler approximations such as the interference model of Eq. (14).

It is worth noting that there is, in principle, no difficulty in making the target a polyatomic molecule. The number of target parameters increases, of course, and it should be well approximated with a one electron potential to use the present approach. A density-functional adaptation might remove this restriction, however. There is also little difficulty in adding an external field. The complexity of the system must in any case be weighed against the overall computational time to achieve the desired goal.

ACKNOWLEDGMENTS

We gratefully acknowledge useful conversations with F. Robicheaux and I. Ben-Itzhak; and we thank M. Koehler for her critical reading of the manuscript. This work was supported in part by the Chemical Sciences, Geosciences and Biosciences Division, Office of Basic Energy Sciences, Office of Science, U.S. Department of Energy, and in part by the Research Corporation.

[1] ALADDIN database, www-amdis.iaea.org/ALADDIN, maintained by J. A. Stephens at the International Atomic Energy Agency (www.iaea.org).
[2] W. Fritsch and C. D. Lin, Phys. Rep. **202**, 1 (1991).
[3] V. Sidis, Adv. At., Mol., Opt. Phys. **26**, 161 (1989).
[4] R. Cabrera-Trujillo, J. R. Sabin, E. Deumens, and Y. Öhrn, Adv. Quantum Chem. **47**, 251 (2004).
[5] A. Kolakowska, M. S. Pindzola, F. Robicheaux, D. R. Schultz, and J. C. Wells, Phys. Rev. A **58**, 2872 (1998).
[6] M. S. Pindzola, T. Minami, and D. R. Schultz, Phys. Rev. A **68**, 013404 (2003).
[7] D. R. Schultz and P. S. Krstić, Phys. Rev. A **67**, 022712 (2003).
[8] I. Reiser, Ph.D. dissertation, Kansas State University, 2002.
[9] I. Reiser and C. L. Cocke, Phys. Rev. A **67**, 062718 (2003).
[10] H. Bräuning, I. Reiser, A. Diehl, A. Theiss, E. Sidky, C. L. Cocke, and E. Salzborn, J. Phys. B **34**, L321 (2001).
[11] M. Kimura, Phys. Rev. A **32**, 802 (1985).
[12] M. Kumura, S. Chapman, and N. F. Lane, Phys. Rev. A **33**, 1619 (1986).
[13] P. S. Krstić, Phys. Rev. A **66**, 042717 (2002); P. S. Krstić and R. K. Janev, *ibid.* **67**, 022708 (2003).
[14] J. Caillat, A. Dubois, I. Sundvor, and J. P. Hansen, Phys. Rev. A **70**, 032715 (2004).
[15] T. F. Tuan and E. Gerjuoy, Phys. Rev. **117**, 756 (1960).
[16] N. C. Deb, A. Jain, and J. H. McGuire, Phys. Rev. A **38**, 3769 (1988).
[17] Y. D. Wang, J. H. McGuire, and R. D. Rivarola, Phys. Rev. A **40**, 3673 (1989).
[18] R. Shingal and C. D. Lin, Phys. Rev. A **40**, 1302 (1989).
[19] R. Shingal and C. D. Lin, J. Phys. B **22**, L659 (1989).
[20] W. H. Press, S. A. Teukolsky, W. T. Vetterling, and B. P. Flannery, *Numerical Recipes*, 2nd ed. (Cambridge University Press, Cambridge, U.K., 1992), p. 640–642.
[21] D. J. Phalen, M. S. Pindzola, and F. Robicheaux Phys. Rev. A (to be published).